Supplement: Molecular Simulations of Liquid Jet Explosions and Shock Waves Induced by X-Ray Free-Electron Lasers

Leonie Chatzimagas and Jochen S. Hub*

Theoretical Physics and Center for Biophysics,

Saarland University, Saarbrücken 66123, Germany

(Dated: September 7, 2023)

SUPPLEMENTARY METHODS

Simulation system setup and heating of the jet

The liquid jet was modeled as a cylinder of water molecules equilibrated at 300 K. The jet was placed into a cubic box with periodic boundary conditions in a vacuum environment. Three water models were used to model the jet: the all-atom models SPC/E [S5] and TIP4P/2005 [S6] and the coarse-grained (non-polarizable) MARTINI water model [S7]. The geometries of atomistic water models were constrained with the SETTLE algorithm [S8]. The energy was minimized using a steepest descent algorithm, and the jet was equilibrated for 25 ps at a temperature of 300 K using the velocity-rescaling thermostat [S9]. The flow of the jet was not modeled whereas, in experiments, the jet travels with a velocity of typically 10 m/s to 100 m/s. We neglected the jet flow in our simulations because the jet velocity is slow compared to the velocities of the shock waves.

We heated the central segment of the jet by assigning new velocities to the water atoms or beads at the jet center drawn from the Maxwell–Boltzmann distribution. Accordingly, new velocities were assigned to every atom j within a cylinder that is orthogonally crossing the water jet. The cylinder radius was taken as $R = 3\sigma$, where σ is the standard deviation of a Gaussian-shaped intensity profile modeling the X-ray pulse. The components $v_{i,j}$ of the new velocity of atom j were drawn from the Maxwell–Boltzmann distribution,

$$P(v_{i,j}) = \sqrt{\frac{m_j}{2\pi k_b T(r)}} \exp\left(-\frac{m_j v_{i,j}^2}{2k_b T(r)}\right) , \tag{1}$$

where m_j is the mass of atom j and k_b the Boltzmann constant. The temperature $T(r)$ was taken as a Gaussian of distance r of atom j from the cylinder axis, orthogonal to the jet:

$$T(r) = (T_{\max} - T_{\mathrm{eq}})\, e^{-\frac{r^2}{2\sigma^2}} + T_{\mathrm{eq}} \tag{2}$$

Hence, the temperature decayed from $T_{\max} = 10^5$ K to the equilibrium temperature $T_{\mathrm{eq}} = 300$ K. The maximum temperature $T_{\max}$ was chosen to match the plasma dynamics simulations by Beyerlein *et al.* [S10].

Simulation parameters for numerically stable NVE simulations

Due to the high temperatures up to 10^5 K and, thus, large velocities, an integration timestep of 0.02 fs was required for obtaining numerically stable simulations with atomistic

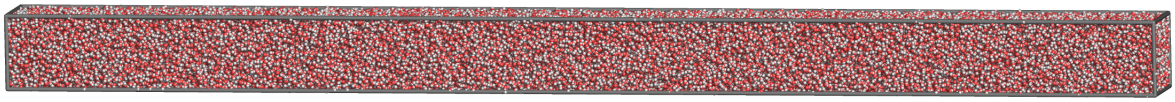

FIG. S1. Simulation box with periodic boundary conditions filled with SPC/E water. The grey lines represent the box edges. The box size is 5 nm × 5 nm × 80 nm.

water models after heating the jet. Because of the small integration timestep, double precision was required in GROMACS to prevent large energy drifts. The decrease of the peak temperature during simulations enabled the use of larger integration time steps at later simulation times; namely, 0.4 fs for 10 nm or 20 nm diameter jets and 0.2 fs for 40 nm diameter jets, respectively, after 0.1 ps. In coarse-grained MARTINI water model simulations, the initial integration timestep was set to 0.4 fs and was increased to 2 fs after 0.1 ps, providing numerically stable simulations.

The methods for computing non-bonded interactions were critical for avoiding large energy drifts in the NVE simulations. The Lennard-Jones interactions were computed using a cut-off with potential shift. The coulomb interactions were computed using the reaction field method with an infinite dielectric constant [S11]. For both methods, the cut-off distance was set to 1.2 nm and the pair-lists were determined with the verlet cut-off scheme. While the particle-mesh Ewald [S12] method likewise prevented an energy drift, it is inefficient for computing interactions in our systems due to the presence of large vacuum volumes.

The geometry of atomistic water molecules were constrained with the SETTLE algorithm to prevent large distortions of water bonds and angles, which would lead to crashes in the simulation.

Statistically independent simulations were carried out by performing a 5 ps NVT simulation at 300 K with a random set of initial velocities, followed by an independent heating of the jet center before each simulation run.

Jet (nm)	Beam (nm)	water model	N	t (ps)
10	1.5	SPC/E	20	50
10	6	SPC/E	18	50
20	3	SPC/E	50	50
20	6	SPC/E	42	50
40	6	SPC/E	19	25
20	3	TIP4P/2005	23	50
20	3	MARTINI	25	100
40	6	MARTINI	20	100
40	9	MARTINI	20	100
60	9	MARTINI	20	100
80	12	MARTINI	20	100

TABLE S1. Summary of the simulation parameters: jet diameter "Jet", FWHM of the modeled X-ray beam "Beam", number of simulations N, simulation time t.

Selection of systems for further analysis

For certain simulation sets, the pressure acting by the vaporized jet center was insufficient for splitting the jet into two segments. Such simulation sets were not considered in the analysis.

Density and temperature analysis

The density in the jet was computed in 200 bins along the jet axis and in 50 bins in radial direction. The density in the box with periodic boundary conditions was averaged over 100 bins distributed along the longest box axes. The density in each bin was averaged over independent simulations. The number of independent simulations for each system is listed in Tab. S1. The temperature T was computed from the averaged kinetic energy $E_{\mathrm{kin}} = \frac{1}{2} N_{\mathrm{df}} k_b T$, where N_{df} are the degrees of freedom of the system. The energy was averaged over the same bins and over the same number of independent simulations as the density in the jet.

Density peak attenuation

To investigate the propagation of the first shock wave, we determined the density peak height in dependence of the distance of the peak position from the jet center for each time frame and simulation set. The one-dimensional densities as function of z and time were obtained by first averaging the two-dimensional densities along radial direction perpendicular to the jet axis up to a distance of a quarter of the jet radius. Thus, the analysis excluded contributions from regions near the jet surface, where the shock front is curved and where the density is reduced owing to surface effects. The density peak height was obtained by interpolating the density along the jet with a cubic spline. Then, two options were used to determine the density peaks: (i) the scipy tool signal.find_peaks was used to find the position and height of the density peaks or (ii) the peak was defined as the maximum density value of the non-interpolated density data. Option (i) was used if possible; however, for larger times, the peaks were wide and noisy leading to over-fitting of the spline interpolation. Thus, if option (i) did not detect a peak, option (ii) was used. Furthermore, the peaks were only accepted if the density was larger than the thresholds of $1005\,\mathrm{kg/m^3}$ and $1050\,\mathrm{kg/m^3}$ for atomistic and MARTINI water models, respectively. The height of the peak, Δ Density, was defined as the difference of the density at the peak relative to the averaged density of the equilibrated jet.

Notably, if the radial averaging of the two-dimensional densities would be carried out up to the jet surface (instead of up to only a quarter of the jet radius, as described above), the obtained shock velocities and decay lengths change considerably. Specifically, the obtained velocities change by 3% to 13% and decay lengths by 6% to 33%. These differences are rationalized by contributions by the curved shock front and the reduced density near the jet surface. Thus, our averaging scheme up to a quarter of the jet radius was chosen with the aim to report the shock wave progression near jet axis.

SUPPLEMENTARY RESULTS

Jet with 10 nm diameter

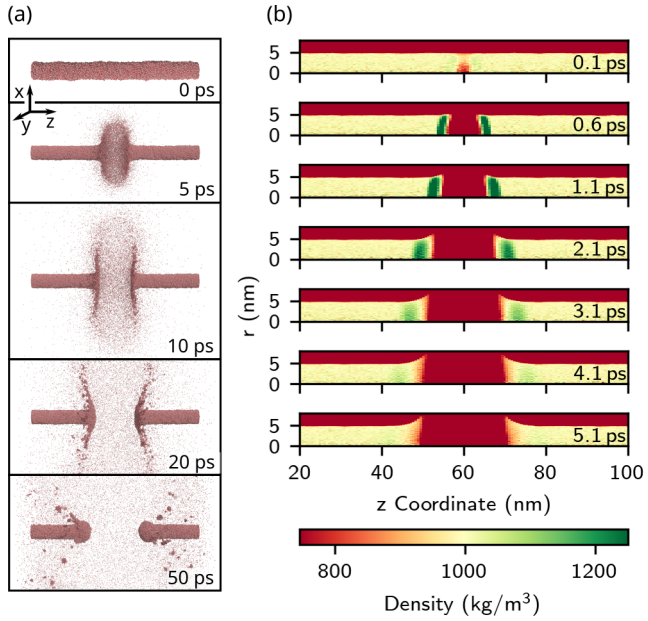

FIG. S2. Simulation of the jet explosion in a water jet with 10 nm diameter induced by a modeled X-ray pulse with 3 nm FWHM. (a) Snapshots of a single simulation. (b) Radial density at 0.1 ps to 5.1 ps after the X-ray impact averaged over 100 independent simulations.

Evolution of the gap size

To analyze the gap growth induced by the jet explosion, we defined the gap as the axial segment with a density below 400 kg/m^3, and we scaled the gap size by the jet diameter (Fig. S3). Notably, the gap size evolution in simulation resembled the evolution in experiments by Stan *et al.* [S1], suggesting that the qualitative gap growth dynamics is conserved over several spatial orders of magnitude. However, in the simulations, the rise of the gap size was delayed by few picoseconds, as required for clearing the central segment after X-ray impact.

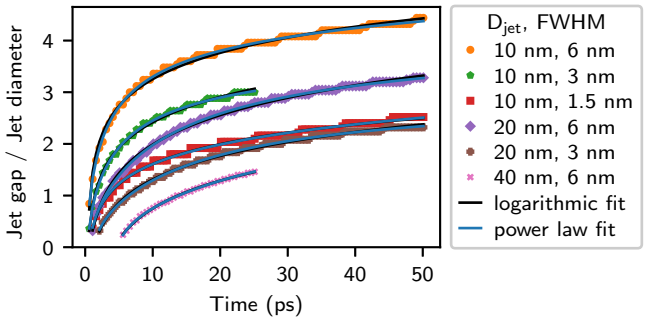

FIG. S3. Evolution of the gap size. The gap was defined as the segment with a density below 400 kg/m^3. The resulting gap size was scaled by the jet diameter and previously proposed models were fitted [S1, S2].

Two models have been put forward to describe the gap growth: a logarithmic growth used by Stan *et al.* [S1] and a power law proposed by Gañán-Calvo [S13]. To test whether these models are compatible with our simulations, we fitted the models to the simulated gap growth, augmented by a delay time before the initial rise of the gap. Accordingly, the logarithmic growth model by Stan *et al.* [S1] was taken as

$$X_{\text{retraction}}/R_{\text{j}} = C \ln(1 + (t - t_0)/\tau), \tag{3}$$

where t_0, C and τ are fitting parameters and R_{j} is the radius of the jet. The power law by Gañán-Calvo [S13] was taken as

$$X_{\text{retraction}}/R_{\text{j}} = C(t - t_0)^{\alpha_0} \left(1 + \left(\frac{t - t_0}{\tau_s}\right)^{\delta}\right)^{(\alpha_1 - \alpha_0)/\delta} \tag{4}$$

$$\alpha_0 = 2/(2 + \gamma) \tag{5}$$

$$\alpha_1 = 5/3 - \gamma \ , \tag{6}$$

Jet (nm)	Beam (nm)	water model	t_0 (ps)	τ (ps)	C
10	1.5	SPC/E	0.6	0.5	5.5
10	3	SPC/E	0.4	0.3	7
10	6	SPC/E	0.4	0.1	7.2
20	3	SPC/E	1.3	1.4	13.4
20	6	SPC/E	0.6	1	16.8
40	6	SPC/E	4.2	3	28.2
20	3	TIP4P/2005	1.1	1.7	14.3
20	3	MARTINI	3.1	1.7	9.9
40	6	MARTINI	5.2	5.1	24.1
40	9	MARTINI	3.3	4.9	29.9
60	9	MARTINI	7	9.9	40.9
80	12	MARTINI	9	15.5	59.4

TABLE S2. Estimated parameters of the logarithmic gap growth model, t_0, τ and C according to Eq. 3. "Jet" denotes jet diameter, and "Beam" denotes the FWHM of the modeled X-ray beam. Uncertainties of fitting parameters t_0, τ and C as provided by the non-linear least squares regression were below 1%.

where t_0, C and τ_s are the fitting parameters of the model and $\gamma = 1.5$ was chosen following Gañán-Calvo [S13].

As shown in Fig. S3, both models are in excellent agreement with the data. However, since the simulation time scales cover less than two orders of magnitude, the data is insufficient to unambiguously determine all parameters in the power law model (Table S3), or to decide whether one of the models is preferable for describing the gap growth. Taken together, the gap growth in simulations agrees with previous experiments and is compatible with the models by Stan *et al.* [S1] and Gañán-Calvo [S13].

Jet (nm)	Beam (nm)	water model	t_0 (ps)	C	τ_s (ps)	δ
10	1.5	SPC/E	0.8	0.7	3.6 ± 0.7	0.95
10	3	SPC/E	0.4	1	6.3 ± 0.6	1.09
10	6	SPC/E	0.3	1.6	3.79 ± 0.07	1.07
20	3	SPC/E	1.4	0.4	29 ± 7	1.18
20	6	SPC/E	0.7	0.6	20 ± 2	1.13
40	6	SPC/E	5	0.3	30 ± 160	0.91 ± 0.03
10	3	TIP4P/2005	1.4	0.4	30 ± 30	1.22 ± 0.18
20	3	MARTINI	3.3	0.3	32 ± 17	1.18
40	6	MARTINI	6.2	0.2	82 ± 24	1.17
40	9	MARTINI	4.1	0.2	92 ± 15	1.25
60	9	MARTINI	9	0.1	170 ± 60	1.39
80	12	MARTINI	12.8	0.2	0.05 ± 0.15	0.45 ± 0.01

TABLE S3. Estimated parameters of the power law gap growth model, t_0, C, τ_s, δ, according to Eq. 6. "Jet" denotes jet diameter, and "Beam" denotes the FWHM of the modeled X-ray beam. Reported uncertainties were taken from the uncertainties of the non-linear least squares regression. Uncertainties of fitting parameters C and δ not reported in the table were below 1%.

Estimate of rate of cavitation bubble nucleation

To rationalize the absence of cavitation bubbles in our simulations of jet explosion (Fig. S4), we estimated the rate of cavity formation following Menzl *et al.* [S14]. Accordingly, in a simulation of a jet explosion with 20 nm diameter induced by a modeled X-ray pulse with 3 nm FWHM, taking a pressure of −165 MPa in a volume of 3140 nm^3, the probability of forming a cavitation bubble within 5 ps is in the order of only 10^{-6}. Thus, cavitation bubbles would be expected only in by far larger simulation systems over longer simulation times.

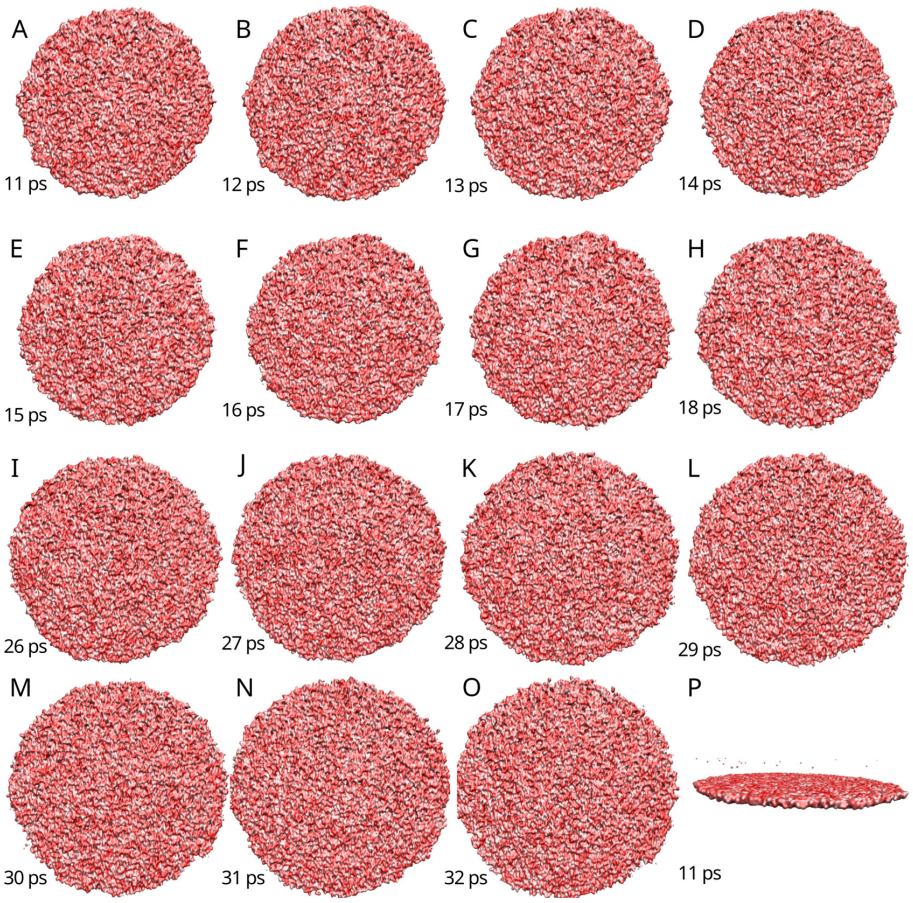

FIG. S4. Slice of 0.5 nm thickness at a distance of 26 nm from the jet center taken from a simulation of a jet with 20 nm diameter and a modeled X-ray pulse of 3 nm FWHM. Water in the slices is shown in surface representation and taken from time delays between 11 ps and 32 ps (see labels). No cavitation bubbles are formed in the simulations, in contrast to the experimental observations in larger jets [S1, S2].

Different combinations of jet diameter and FWHM of the modeled X-rays pulse

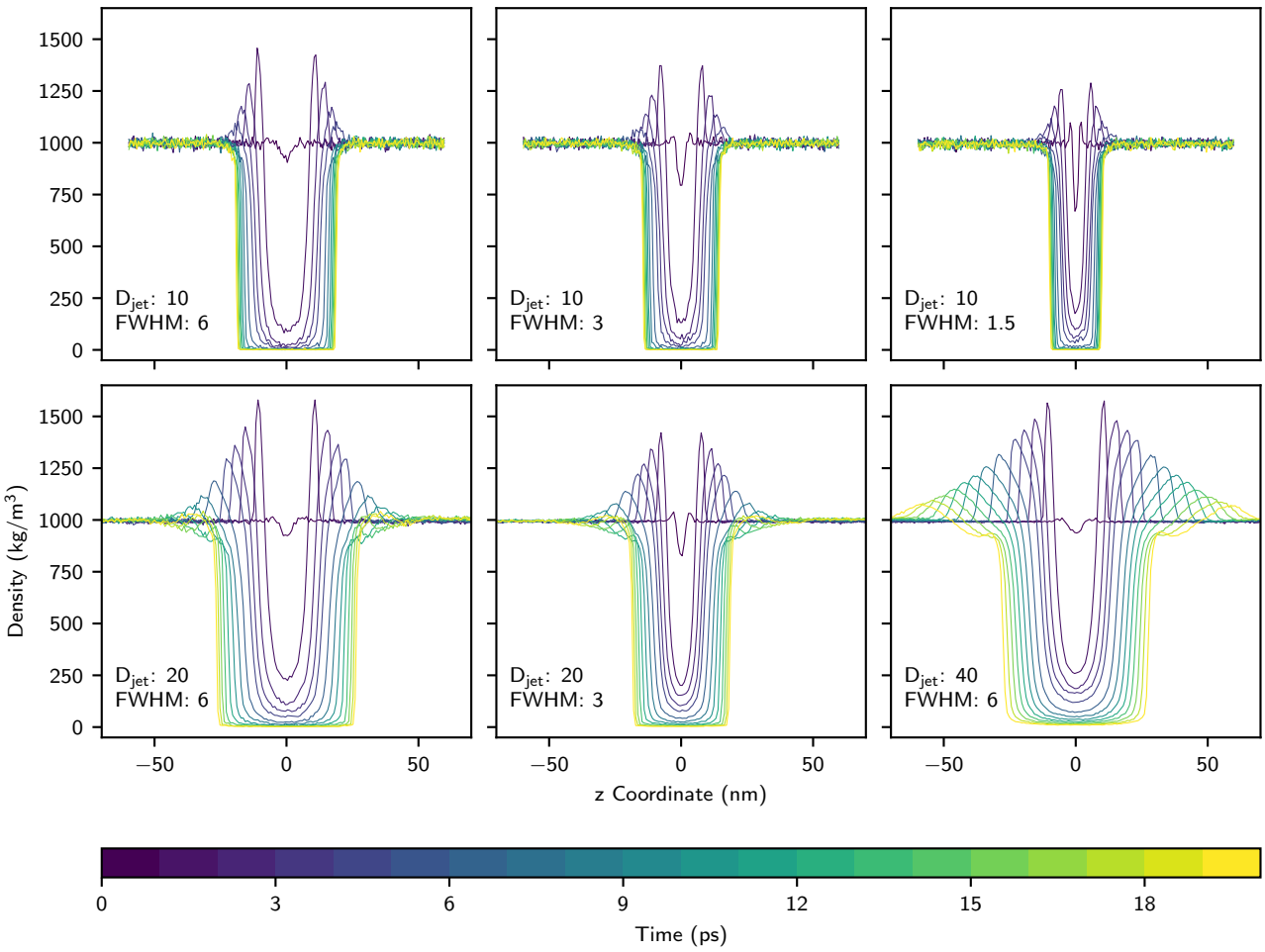

FIG. S5. Time evolution of the water density for simulations with different combinations of water jet diameter, D_{jet}, and FWHM of the modeled X-rays pulse. D_{jet} and FWHM in nanometer are listed in panels. The densities reveal slower shock wave decay with larger D_{jet} and higher density peaks with increased FWHM, leading to increased deposited energy.

Parameters of shock wave propagation and attenuation in jets

Jet (nm)	Beam (nm)	water model	v_S (km/s)	τ_{dec} (nm)	m_{log}
10	1.5	SPC/E	2.21 ± 0.04	4.6	-2.2
10	3	SPC/E	2.44 ± 0.01	4.1	-2.4
10	6	SPC/E	2.21 ± 0.03	4.1	-2.5
20	3	SPC/E	2.199 ± 0.002	8.3	-2.4
20	6	SPC/E	2.113 ± 0.002	8.7	-2.3
40	6	SPC/E	2.011 ± 0.001	20.6	-1.9
20	3	TIP4P/2005	2.06	7.9	-2.5
20	3	MARTINI	2.293 ± 0.005	12.8	-1.6
40	6	MARTINI	2.358 ± 0.001	21.9	-1.8
40	9	MARTINI	2.5	26.4	-1.5
60	9	MARTINI	2.374 ± 0.002	34.6	-1.7
80	12	MARTINI	2.195	62.1	-1.3

TABLE S4. Estimated parameters of the shock wave propagation and attenuation: jet diameter "Jet", FWHM of the modeled X-ray beam "Beam", velocity of the first shock wave v_S, decay length τ_{dec} and the slope of the log-linear fit to the scaled density decay m_{log} (3(a), S8(a), S10(a)). Uncertainties of m_{log} as reported by least squares regression were below 3%.

Shock dynamics in box with periodic boundary conditions

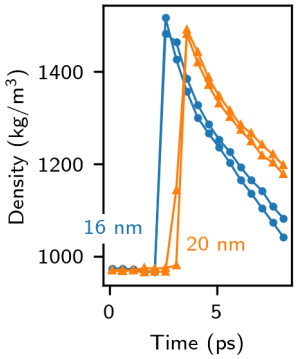

FIG. S6. Time evolution of the density peak resulting from a shock induced in a box with periodic boundary conditions (Fig. S1) by instantaneous heating of the central box segment with a peak temperature of 100 000 K. Densities were taken at distances of 16 nm (blue) or 20 nm (orange) from the box center. The density profiles are characterized by a sharp increase followed by a gradual decay, as common for shock waves (or blast waves) in bulk media [S3]. Notably, compared to the shock wave in the jet, the density peak is by far higher, the density shape differs, and the shock travels faster (cf. Fig. S7 and Table S5).

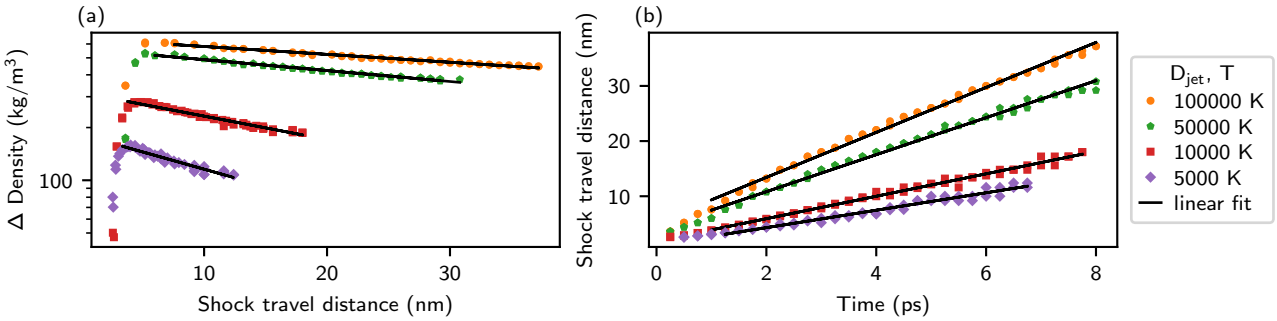

FIG. S7. Shock wave attenuation and propagation in a box with periodic boundary conditions using the SPC/E water model and different maximum temperatures of 100 000 K, 50 000 K, 10 000 K, and 5000 K. (a) Density peak attenuation of the shock wave. (b) Propagation of shock waves with approximately constant velocities within the observed time range. Velocities are in good agreement with the experimental data by Rice and Walsh [S4] as shown in Table S5, suggesting that SPC/E is capable of modeling shock waves with reasonable accuracy.

T (K)	N	t (ps)	v_{S} (km/s)	$1/\rho$ (cm^3/g)	U_s (km/s) [S4]	τ_{dec} (nm)	$m_{\log}$
100000	50	40	4.078 ± 0.017	0.678	3.91	96.4	-0.01
50000	20	40	3.354 ± 0.015	0.715	3.273	69.7	-0.14
10000	20	40	2.034 ± 0.007	0.835	2.008	32.4	-0.03
5000	20	40	1.583 ± 0.019	0.911	$<$2.008	22	-0.05

TABLE S5. Summary of the simulation parameters and results of the shock wave propagation in a water-filled box with periodic boundary conditions: maximum temperature T used to induce the shock wave, number of simulations N, simulation time t, velocity of the shock wave v_{S}, inverse density $1/\rho$ at the peak for comparison with Table III by Rice and Walsh [S4], experimental shock velocity U_s as expected from $1/\rho$ according to Rice and Walsh, decay length τ_{dec}, and the slope of the log-linear fit to density decay $m_{\log}$ (cf. Fig. S7(a)). Uncertainties of $m_{\log}$ reported by least squares regression were below 2.5%. Notably, the shock velocities in simulations v_S are in good agreement with the velocities U_s by Rice and Walsh, suggesting that SPC/E is capable of modeling shock waves with reasonable accuracy. The decay length with 100 000 K in the PBC box (top column) is by far longer as compared to the decay lengths in the jet (Table S4, SPC/E water model), in which the shock waves were likewise induced with a maximum temperature of 100 000 K.

Influence of water model and atomic details

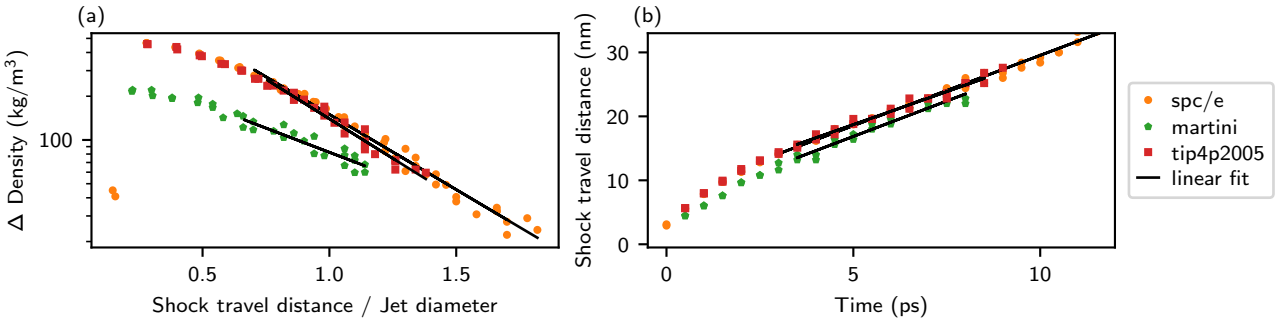

FIG. S8. Comparison of shock wave attenuation and propagation using the atomistic three-site SPC/E model (orange), the atomistic four-site TIP4P/2005 model (red), or the coarse-grained MARTINI water model (green), modeling the water as Lennard-Jones fluid. The densities were calculated from simulations of water jets with 20 nm diameter after explosion induced by a modeled X-rays pulse with 3 nm FWHM. Using different water models lead to qualitatively similar attenuation and propagation dynamics. (a) Density peak attenuation of the leading shock wave scaled by the water jet diameter. The relative height of the density peaks, Δ Density, attenuates with the propagation distance to the jet center. The linear attenuation on the semi-log plot indicates an exponential decay of the density. Results from TIP4P/2005 and SPC/E are nearly in quantitative agreement. In contrast, MARTINI leads to slower density decay. (b) Propagation of the first shock wave. The shock waves propagate with constant, supersonic velocity after few picoseconds regardless of the choice of the water model.

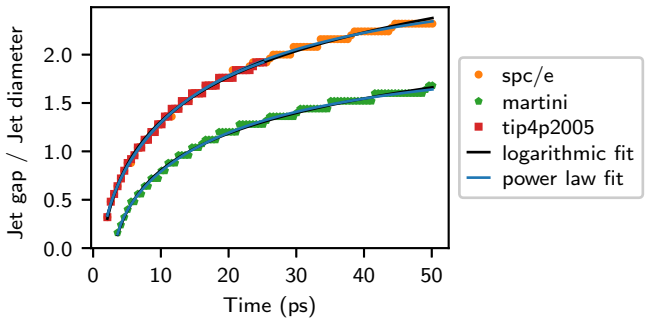

FIG. S9. Evolution of the gap sizes using the atomistic three-site SPC/E (orange) and four-site TIP4P/2005 (red) water models as well as the coarse-grained MARTINI water model (green). The gap size was calculated from simulations of a water jet with 20 nm diameter after explosion induced by a modeled X-rays pulse with 3 nm FWHM. Different water models lead to qualitatively similar gap size evolution. However, while the two atomistic water models lead to nearly indistinguishable gap size evolutions, the MARTINI water model leads to a slower gap growth. Lines indicate fitted models of gap growth [S1, S2].

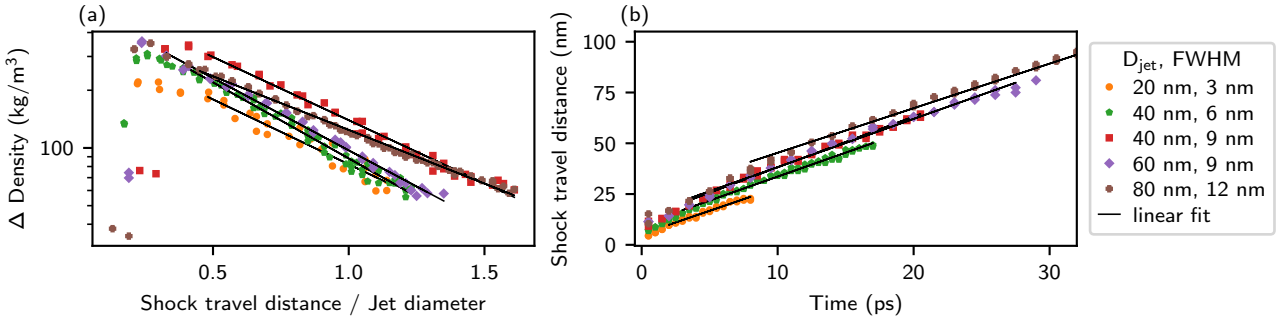

FIG. S10. Shock wave attenuation and propagation using the MARTINI model. (a) Density peak attenuation of the leading shock wave scaled by the water jet diameter. The relative height of the density peaks, Δ Density, attenuates with the propagation distance to the jet center. The linear attenuation on the semi-log plot indicates an exponential density decay. The attenuation scales approximately with jet diameter. (b) Propagation of the first shock wave with constant, supersonic velocity of approximately 2210 m/s after few picoseconds (see also Table S1).

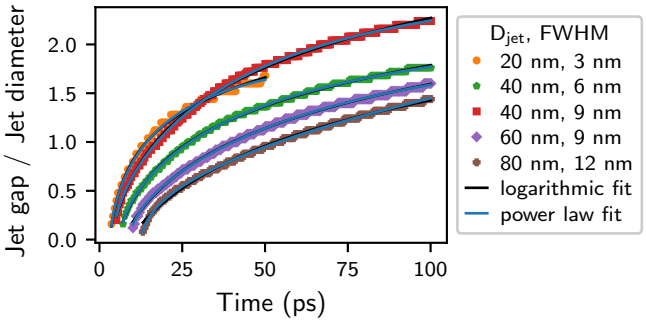

FIG. S11. Evolution of the gap size using the MARTINI model for systems with different jet diameters and X-ray pulse FWHM (colored symbols, see legend), qualitatively similar to results with SPC/E (cf. Fig. S3). The resulting gap size was scaled by the jet diameter. Previously proposed models [S1, S2] were fitted to the data (lines).

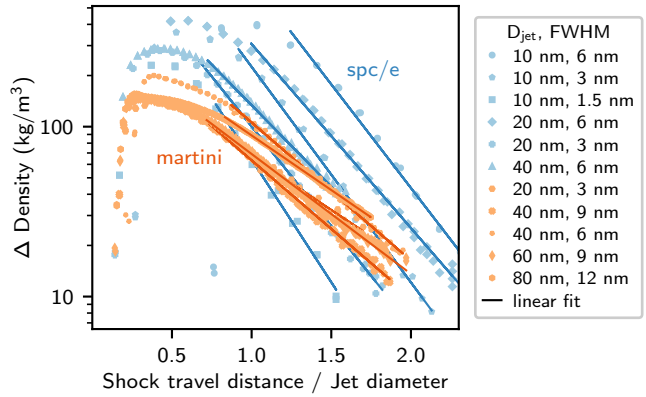

FIG. S12. Influence of atomistic details on the density peak attenuation, where the density used to determine the peaks was averaged over the entire cross section of the jet. The density decays over shorter distances when using the atomistic SPC/E model (blue) as compared to using the coarse-grained MARTINI water model (orange). This difference in decay length is more pronounced as compared to Figure 4, for which the density was averaged only within the innermost quarter of the jet radius.

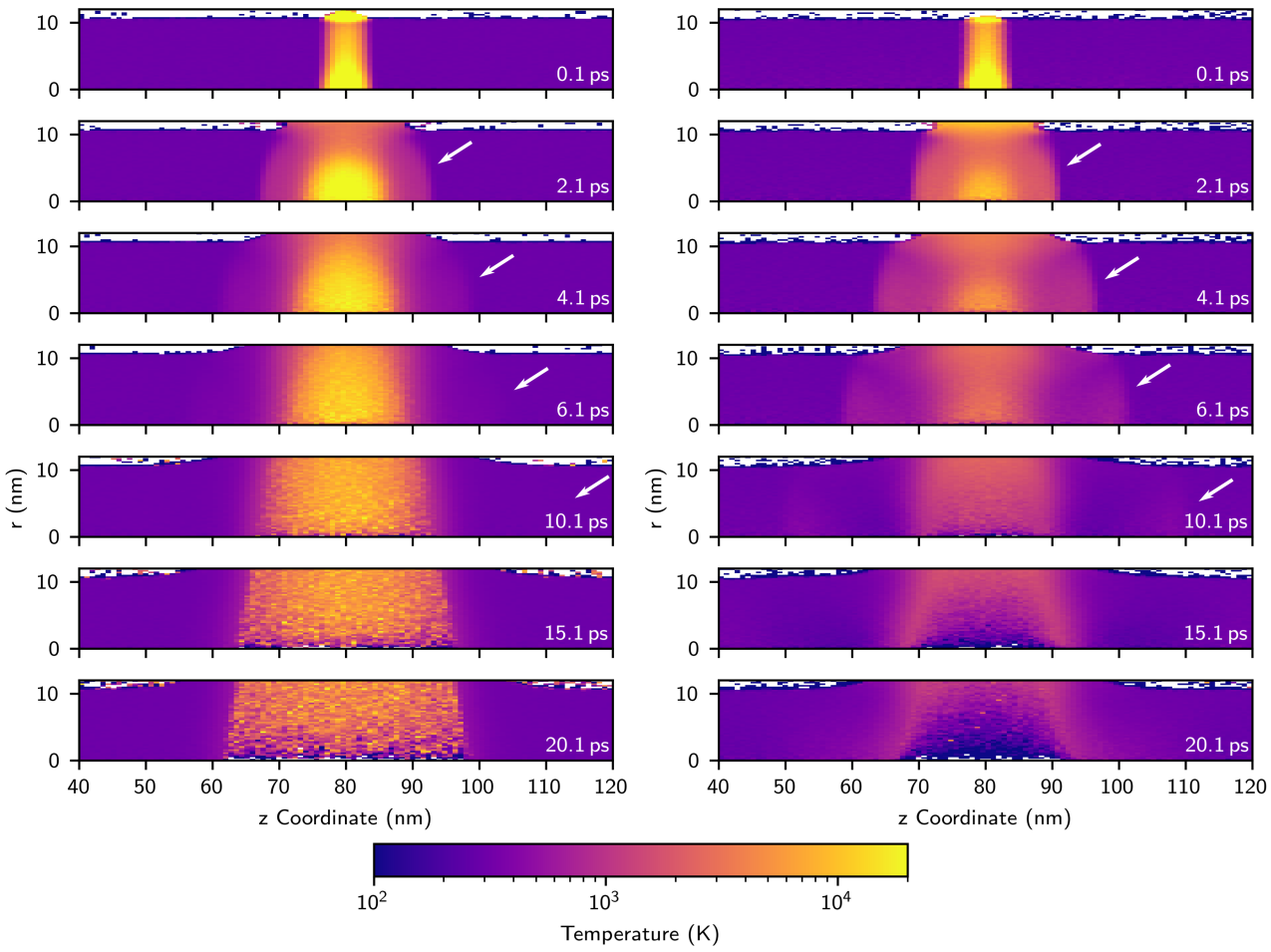

FIG. S13. On the influence of atomistic details on the time evolution of the temperature in a water jet with 20 nm diameter after explosion induced by a modeled X-ray pulse with 3 nm FWHM averaged over 20 simulations. Panels show the spatial distribution of temperature along the jets at time delays between 0.1 ps and 20.1 ps (see labels). The energy transported by the shock wave is increased and decays more slowly when using the coarse grained MARTINI water model (right) as compared to using the SPC/E model (left), as revealed by the propagating shock fronts highlighted by white arrows.

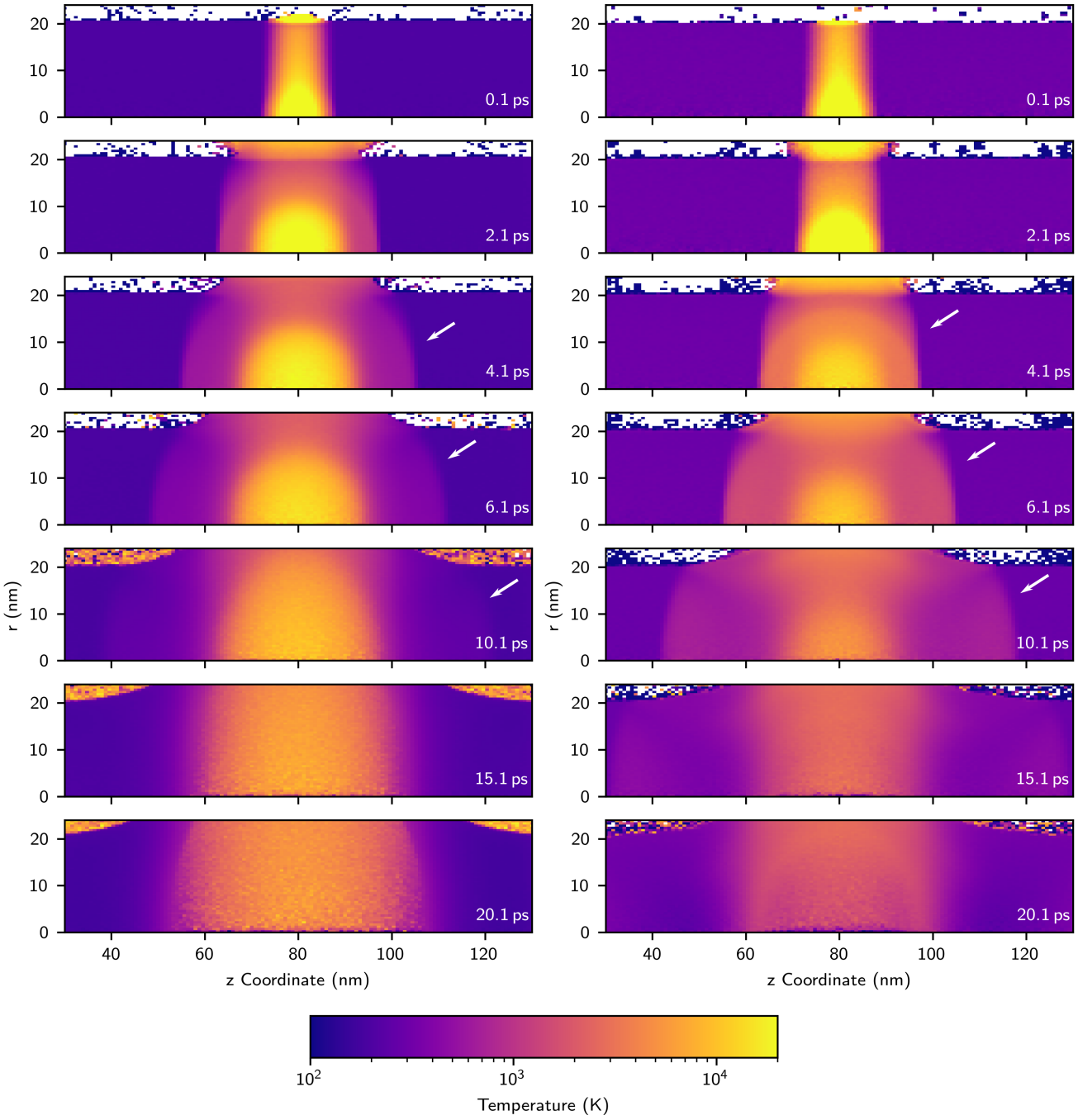

FIG. S14. On the influence of atomistic details on the time evolution of the temperature in a water jet with 40 nm diameter after explosion induced by a modeled X-ray pulse with 6 nm FWHM averaged over 20 simulations. Panels show the spatial distribution of temperature along the jets at time delays between 0.1 ps and 20.1 ps (see labels). The energy transported by the shock wave is increased and decays more slowly when using the coarse-grained MARTINI water model (right) as compared to using the SPC/E model (left), as revealed by the propagating shock fronts highlighted by white arrows.

* jochen.hub@uni-saarland.de

[S1] C. A. Stan, D. Milathianaki, H. Laksmono, R. G. Sierra, T. A. McQueen, M. Messerschmidt, G. J. Williams, J. E. Koglin, T. J. Lane, M. J. Hayes, *et al.*, Nat. Phys. **12**, 966 (2016).

[S2] G. Blaj, M. Liang, A. L. Aquila, P. R. Willmott, J. E. Koglin, R. G. Sierra, J. S. Robinson, S. Boutet, and C. A. Stan, Phys. Rev. Fluids **4**, 043401 (2019).

[S3] N. Abdul-Karim, C. S. Blackman, P. P. Gill, E. M. M. Wingstedt, and B. A. P. Reif, RSC Adv. **4**, 54354 (2014).

[S4] M. H. Rice and J. M. Walsh, J. Chem. Phys. **26**, 824 (1957).

[S5] S. Chatterjee, P. G. Debenedetti, F. H. Stillinger, and R. M. Lynden-Bell, J. Chem. Phys. **128**, 124511 (2008).

[S6] J. L. Abascal and C. Vega, J. Chem. Phys. **123**, 234505 (2005).

[S7] S. J. Marrink, H. J. Risselada, S. Yefimov, D. P. Tieleman, and A. H. De Vries, J. Phys. Chem. B **111**, 7812 (2007).

[S8] S. Miyamoto and P. A. Kollman, J. Comput. Chem. **13**, 952 (1992).

[S9] G. Bussi, D. Donadio, and M. Parrinello, J. Chem. Phys. **126**, 014101 (2007).

[S10] K. R. Beyerlein, H. O. Jönsson, R. Alonso-Mori, A. Aquila, S. Bajt, A. Barty, R. Bean, J. E. Koglin, M. Messerschmidt, D. Ragazzon, *et al.*, Proc. Natl. Acad. Sci. U. S. A. **115**, 5652 (2018).

[S11] D. Van Der Spoel and P. J. van Maaren, J. Chem. Theory Comput. **2**, 1 (2006).

[S12] T. Darden, D. York, and L. Pedersen, J. Chem. Phys. **98**, 10089 (1993).

[S13] A. M. Gañán-Calvo, Phys. Rev. Lett. **123**, 064501 (2019).

[S14] G. Menzl, M. A. Gonzalez, P. Geiger, F. Caupin, J. L. Abascal, C. Valeriani, and C. Dellago, Proc. Natl. Acad. Sci. U.S.A. **113**, 13582 (2016).